Multiple mechanisms disrupt the *let-7* microRNA family in neuroblastoma

John T Powers[1], **Kaloyan M Tsanov**[1], **Daniel S Pearson**[1], **Frederik Roels**[4], **Catherine S Spina**[2], **Richard Ebright**[1], **Marc Seligson**[1], **Yvanka de Soysa**[1], **Patrick Cahan**[1], **Jessica Theiβen**[4], **Ho-Chou Tu**[1], **Areum Han**[1], **Kyle C Kurek**[3], **Grace S LaPier**[1], **Jihan K Osborne**[1], **Samantha J Ross**[1], **Marcella Cesana**[1], **James J Collins**[2], **Frank Berthold**[4], and **George Q Daley**[1,*]

[1]Division of Pediatric Hematology/Oncology, Stem Cell Transplantation Program, Howard Hughes Medical Institute, Boston Children's Hospital and Dana Farber Cancer Institute; Department of Biological Chemistry and Molecular Pharmacology, Harvard Medical School; Broad Institute; Boston, MA 02115, USA Harvard Stem Cell Institute, Boston, MA 02115, USA

[2]Department of Biological Engineering, Massachusetts Institute of Technology; Broad Institute of MIT and Harvard; Wyss Institute for Biologically Inspired Engineering; Boston, MA 02115, USA

[3]Department of Pathology, Boston Children's Hospital, Boston MA 02215, USA

[4]Department of Pediatric Oncology, University Hospital Koln, Cologne, Germany

Abstract

Poor prognosis in neuroblastoma is associated with genetic amplification of *MYCN*. *MYCN* is itself a target of *let-7*, a tumor suppressor family of microRNAs implicated in numerous cancers. *LIN28B*, an inhibitor of *let-7* biogenesis, is overexpressed in neuroblastoma and has been reported to regulate *MYCN*. However, here we show that *LIN28B* is dispensable in *MYCN*-amplified neuroblastoma cell lines, despite de-repression of *let-7*. We further demonstrate that *MYCN* mRNA levels in amplified disease are exceptionally high and sufficient to sponge *let-7*, which reconciles the dispensability of *LIN28B*. We found that genetic loss of *let-7* is common in neuroblastoma, inversely associated with *MYCN*-amplification, and independently associated with poor outcomes, providing a rationale for chromosomal loss patterns in neuroblastoma. We propose

that *let-7* disruption by *LIN28B*, *MYCN* sponging, or genetic loss is a unifying mechanism of neuroblastoma pathogenesis with broad implications for cancer pathogenesis.

Carcinogenesis involves multiple genetic and epigenetic events, yet the organizing principles underlying their choreography are poorly understood. MicroRNA (miRNA) deregulation is an important component of this landscape through both oncogenic and tumor suppressive functions of miRNAs[1]. Of these, the highly conserved *let-7* family has a prominent role in the regulation of embryonic development and maintenance of differentiated tissues and is among the most abundantly expressed miRNAs. It serves as a potent tumor suppressor via post-transcriptional repression of multiple oncogenic mRNA targets including *RAS*, *MYC*, and *HMGA2*[2–4]. *Let-7* is downregulated in multiple tumor types and has been causally linked to oncogenesis[1,5–8]. Uncovering the mechanisms by which *let-7* function is neutralized is therefore critical to both the fundamental understanding of cancer pathogenesis and novel therapies.

Several mechanisms of *let-7* disruption have emerged in different contexts. First, its biogenesis can be suppressed by the *LIN28B* RNA-binding protein[9]; a highly conserved heterochronic gene implicated in cancer and reported to induce tumors in multiple mouse models including hepatocellular carcinoma, colon cancer, Wilms' tumor, and neuroblastoma[10–16]. Second, competing endogenous RNAs (ceRNAs) have been proposed to sponge miRNAs, including *let-7*, diluting their activity through competition for miRNAs with sites common to multiple ceRNA species[17–19]. Third, chromosome loss is a suggested mechanism of *let-7* disruption in cancer, as genetic deletion of *let-7* is associated with several solid tumors[1].

The neuroblastoma master oncogene, *MYCN*, has a 910 nucleotide long 3′UTR containing two *let-7* binding sites which are almost perfectly conserved among land vertebrates, suggesting strong functional relevance[20–22] (ED 1). Coding sequence mutations in neuroblastoma are rare[23,24], whereas chromosome arm gain or loss events are common[25,26]. The most well-known chromosomal aberration is amplification of the *MYCN* locus, which occurs in ~25% of all neuroblastomas and largely defines poor prognosis[27,28]. Other common chromosomal deletions at chromosome arms 3p and 11q are inversely associated with *MYCN*-amplification. The reason for this discordance is unknown.

Here, we set out to understand the relationship between *MYCN* and *let-7* in neuroblastoma. A complex relationship emerged between *LIN28B* activity, a novel ceRNA function of the *MYCN* 3′UTR, and *let-7* genetic loss, which together present a unifying model of *let-7* suppression during neuroblastoma pathogenesis. This model provides an organizing principle for understanding distinct genetic patterning in neuroblastoma, with potential implications for cancer in general.

LIN28B and let-7 regulate the MYCN 3′UTR

LIN28B is highly expressed in human neuroblastoma and its expression correlates with tumor stage, rendering the *LIN28B/let-7* axis an attractive target for interrogation (ED 2 a, b, c, d). Two recent reports concluded that this pathway plays a critical role in regulating

MYCN and neuroblastoma cell growth[12,13]. To examine the relationship between the *MYCN* transcript, *let-7* and *LIN28B,* we first transfected non-*MYCN* amplified neuroblastoma cells with the *MYCN* open reading frame, with or without the 3′ UTR carrying intact or mutant *let-7* sites (fig. 1a). The full-length wildtype *MYCN* transcript produced markedly lower MYCN protein levels than the ORF-only construct. Mutation of the *let-7* sites in the 3′ UTR partially rescued MYCN expression, implicating *let-7* modulation as an important component of *MYCN* post-transcriptional regulation (fig. 1b). Expression of *LIN28B* suppressed the *let-7* family in non-*MYCN*-amplified neuroblastoma cells and conferred a growth advantage. *LIN28B* rescued expression of the wildtype 3′ UTR construct, demonstrating that *LIN28B* can support *MYCN* expression through *let-7* repression in the absence of *MYCN* amplification (ED 2e, 2f, fig. 1c). However, when we transfected *MYCN*-amplified cells with a *let-7a* mimic, we observed decreased MYCN protein levels only above 15 and 80 fold increases in cellular levels of *let-7a*, respectively, suggesting that *MYCN* was refractory to all but exceedingly high levels of exogenous *let-7* (fig. 1d).

LIN28B is dispensable in *MYCN*-amplified neuroblastoma cell lines

Next, we evaluated the previously reported *LIN28B-let-7-MYCN* regulatory circuit using published lentiviral shRNA constructs to knockdown *LIN28B* in *MYCN*-amplified neuroblastoma cells and observed comparable suppression of MYCN protein levels and cell growth (ED 3a,b). We further observed reduced xenograft tumor growth in cells expressing a *LIN28B* targeting shRNA (ED 3c). However, we did not observe an appreciable de-repression of *let-7* levels upon shRNA-mediated *LIN28B* knockdown, which is counter to the established paradigm (ED 3d). Moreover, we were unable to rescue these effects through overexpression of shRNA-resistant *LIN28B* constructs (ED 3e,f). Together, these data suggest that the reported effects of the shRNAs on both cell growth and MYCN protein levels might be due to hairpin-induced toxicities.

As an alternative approach to depleting *LIN28B*, we tested five small interfering RNAs (siRNAs) and found that four both effectively knocked down *LIN28B* and, as expected, de-repressed *let-7* levels (ED 4a–d). Upon extended serial siRNA transfection, we observed that despite robust *LIN28B* knockdown and strong de-repression of *let-7*, MYCN protein levels were unaffected and there was no appreciable effect on cell proliferation (ED 4e–g).

To rule out the possibility of incomplete knockdown resulting in residual *LIN28B* activity, we employed *Cas9* and four distinct gRNAs targeting *LIN28B* (ED 4h). We observed robust loss of LIN28B protein with all four gRNA constructs (fig 2a,b), indicating efficient disruption of the locus. We did not observe appreciable loss of MYCN protein expression or impaired cell growth, thus corroborating our siRNA based results (fig. 2a–d). In addition, the *let-7* family was robustly de-repressed, consistent with the existing *LIN28B/let-7* paradigm (fig. 2e,f). These observations indicate that disruption of *LIN28B* has little net impact on *MYCN*-amplified neuroblastoma cells.

MYCN is a *let-7* sponge in *MYCN*-amplified neuroblastoma

The persistence of MYCN protein levels despite high levels of transfected *let-7a* or robust de-repression of *let-7* upon *LIN28B* loss prompted us to explore novel mechanisms of *let-7* perturbation. We hypothesized that there might be a ceRNA in *MYCN*-amplified neuroblastoma cells that serves to sponge *let-7*. To identify potential ceRNAs, we performed poly-A selected RNA-sequencing (mRNA-seq) on *MYCN*-amplified (BE(2)C and Kelly) and non-*MYCN*-amplified (SH-SY5Y) cells. We then determined the relative contribution of *let-7* target sites provided by expressed *let-7* targets. Interestingly, *MYCN* itself was by far the most abundant *let-7* target mRNA in both BE(2)C and Kelly cells, alone providing 19.3% and 18.5% of the entire cellular *let-7*-target-site pool, respectively. In contrast, *MYCN* represented only 0.15% of the *let-7*-target-site pool in SH-SY5Y cells (fig. 3a). In fact, *MYCN* mRNA was the 2nd highest expressed mRNA in both BE(2)C and Kelly cells as opposed to the 5409th highest in SH-SY5Y, demonstrating an exceptionally high *MYCN* mRNA level in *MYCN*-amplified cells (>100-fold increase; fig. 3b). Other multiple-*let-7*-site mRNAs such as *HMGA2*, *IMP1*, and *ARID3B* were expressed at much lower levels, together suggesting that *MYCN* mRNA might itself be the sponge (ED 5a). This expression pattern was validated by qPCR in a panel of additional cell lines (ED 5b).

CeRNA relationships were initially defined in part by similar expression levels between RNAs with similar 3′UTRs[18,29]. Two recent reports have refined this original precept, suggesting that for a given miRNA family, the miRNA: mRNA-target ratio is a major determinant of how effectively a ceRNA can impact the function of a miRNA family. At low ratios, miRNAs are sensitive to moderate levels of ceRNAs, whereas highly expressed miRNAs with high ratios are difficult to sponge, requiring very high levels of ceRNA[30,31]. We therefore assessed total copies per cell of both *MYCN* mRNA and the *let-7* family in BE(2)C and Kelly cells through quantified mRNA-seq and small-RNA sequencing (sRNA-seq) (ED6).

We calculated 13,255 and 10,615 *MYCN* mRNA copies per BE(2)C and Kelly cell, respectively, resulting in 26,511 and 21,231 *let-7* target sites provided by *MYCN* (fig. 3c upper panel). In stark contrast, there were only 31 *MYCN* transcripts per SH-SY5Y cell. Quantification of the *let-7* family in BE(2)C and Kelly cells yielded 7,259 and 1,952 total *let-7* molecules per cell (fig. 3c lower panel), and *MYCN-let-7*-site: *let-7* miRNA ratios of 3.65 and 10.88, respectively. These ratios satisfy the tenets of the ratio-based ceRNA model and do so as the result of a single amplified mRNA. Interestingly, *let-7a* was the most highly expressed *let-7* family member in both cell types, accounting for over half of all *let-7* molecules. These observations were confirmed by spike-in qPCR based quantification of both *MYCN* and *let-7* (ED 7a, b). Even upon *LIN28B* knockout, the *MYCN-let-7*-site: *let-7* ratio is 1.35 in BE(2)C and 1.78 in Kelly, which remain favorable for ceRNA activity (ED 7c).

To test the capacity of *MYCN* mRNA to serve as a *let-7* sponge, we co-transfected BE(2)C cells with a series of luciferase constructs containing the 3′UTRs of several representative *let-7* targets and control or *MYCN* ORF targeting siRNA (ED 8a,b). Luciferase ratios of all constructs save for empty vector controls and the *let-7*-site-mutated *MYCN*-3′UTR, were

significantly reduced by either *MYCN* knockdown or *let-7a* transfection (fig. 3d), suggesting that the endogenous *MYCN*-3′UTR sponges steady-state levels of *let-7*. We then tested the sufficiency of the *MYCN*-3′UTR to de-repress *let-7* targets through sponging of a *let-7a* mimic. We co-transfected the above luciferase reporter constructs with chimeric *RFP:MYCN*-3′UTR constructs and assayed luciferase activity (ED 8c,d). *Let-7* target constructs were rescued when co-transfected with wildtype but not *let-7*-site-mutant *MYCN*-3′UTR (ED 8e). In addition, exogenous *MYCN*-3′UTR was sufficient to enhance MYCN protein expression itself in SK-N-AS cells (ED 8f).

We next tested if endogenous *let-7* targets are sponged. Upon *MYCN* knockdown, protein levels of DICER1, HK2, IMP1, and LIN28B were reduced, while neither mRNA nor *let-7* levels were significantly changed (ED 8a, b, c). Concurrent *let-7* inhibition rescued expression of the four targets, supporting post-transcriptional suppression through *let-7* upon *MYCN* knockdown that is consistent with *MYCN* mRNA serving as a *let-7* sponge (ED 8a). Further, these targets were not reduced at the protein level upon *LIN28B* knockout, which is consistent with this model (ED 8d).

Lastly, we analyzed global *let-7* target expression in response to depletion of the endogenous *MYCN* 3′UTR. To specifically assess the role of the 3′UTR, we transfected BE(2)C cells expressing a *MYCN* ORF transgene with a *MYCN* 3′UTR-targeting siRNA (fig. 3e). While we did not see a global reduction of *let-7* targets as a whole (ED 9e), we did observe significantly lower expression of *let-7* targets with 3 or more total sites or more than one 8mer *let-7* site in their 3′ UTRs, which together define the most sensitive *let-7* targets[32,33] (fig. 3f). Given the regulation of the *MYCN* 3′ UTR by multiple miRNAs[34] and unknown kinetics of how *let-7* activity is restored after the removal of a ceRNA, we further challenged siCon and si*MYCN* cells with a modest amount of *let-7a* mimic, increasing cellular *let-7* levels approximately 8 fold (ED 9f). We then observed significantly reduced expression across all categories of *let-7* targets in si*MYCN* cells, consistent with increased sensitivity to *let-7* in the absence of the *MYCN* 3′ UTR. (fig. 3g, ED 9g).

Let-7 chromosomal loss in neuroblastoma

While neuroblastoma has a low mutation rate, chromosome arm gain and loss is frequent[23,24]. Two of the most common chromosomal losses in neuroblastoma, chromosome arm 3p (Chr3p, ~33% incidence) and Chr11q (~45% incidence), often occur together and seldom with *MYCN*-amplification[23,35,36] (fig. 4a, ED 10). Upon analysis of Chr3p and Chr11q, we noted that the Chr3p-loss smallest region of overlap (SRO) spans from 3p25.3 to 3p14.3[37], placing *let-7g* within the SRO and resulting in its loss whenever Chr3p is lost. In addition, the most common breakpoint of Chr11q immediately proximal to the *let-7a2* locus, resulting in loss of *let-7a2* in virtually all Chr11q deletions[35] (fig. 4b). Moreover, loss of Chr11q in neuroblastoma results in lower overall *let-7a* levels despite loss of only one of three distinct *let-7a* loci[38]. These observations suggest that *let-7* genetic disruption may be selected for in neuroblastoma.

A model in which amplified *MYCN* sequesters mature *let-7* in would predict that selective pressure to genetically lose *let-7* might be relieved in *MYCN*-amplified disease. Chr3p

(*let-7g*) and Chr11q (*let-7a2*) loss patterns are indeed consistent with such a model. To investigate whether the extended *let-7* family (fig. 4b) follows this loss pattern, we expanded our analysis to all eight *let-7* genetic loci in 202 neuroblastomas by array comparative genomic hybridization (aCGH). We created a heat-map of copy number (CN) estimates for each miRNA locus to compare *MYCN*-amplified CN values to non-amplified and observed a significant CN difference for six *let-7* loci (fig. 5a, 5b upper panel). At least one *let-7* family member was lost in 63.4% of non-amplified tumors and in only 16.7% of amplified (fig. 5b upper panel), resulting in average *let-7* CN changes of −1.94 and −0.36 per tumor, respectively (fig. 5b lower panel). This pattern of CN loss for *let-7* is distinct from the unrelated *miR-103a* family (fig. 5b), suggesting that the *let-7* pattern is not reflective of general chromosomal patterning.

Let-7a2, *let-7f2*, and *let-7g* were most commonly lost, whereas *let-7a3/7b* and *let-7i* were not significantly lost in any tumor subset. We reasoned that loss frequency might relate to initial expression level. To interrogate this possibility, we used publicly available sRNA-seq data to examine the relative expression levels of mature *let-7* in twelve distinct primary and tumor cell lines that have intact *let-7* loci (ED 10b). We observed that *let-7a*, *let-7f*, and *let-7g* are present at higher relative levels than other *let-7* family members, which mirrors the CN loss patterns in non-*MYCN*-amplified neuroblastoma (fig. 5c). *MiR-100*, the miRNA-cluster partner of *let-7a2*, is more highly expressed than most *let-7s* and their cluster partners, suggesting that the bulk of the *let-7a* reads may come from the *let-7a2*/*miR-100* locus (fig. 5c).

A limitation of sRNA-seq is that it cannot distinguish between loci that produce the same mature miRNA. *Let-7* family members are coordinately transcribed as part of larger host transcripts (HTs) from which they are then processed, which allows for locus-specific expression analysis[7,39,40] (ED 10c). We therefore analyzed relative expression levels of *let-7* HTs in six primary and tumor cell lines. HT levels for *let-7a2*, 7*f2*, and 7*g* were significantly higher than other *let-7* HTs (ED 10d, fig. 5d), reflecting the pattern of most frequent locus loss in non-amplified disease. In addition, analysis of existing human neuroblastoma mRNA-seq and microarray datasets revealed lower expression of the *let-7a2*, *let-7f2*, and *let-7g* HTs in non-amplified *vs. MYCN*-amplified tumors, which is consistent with observed patterns of CN loss in our aCGH dataset (fig. 5e, ED 10e). Further, *MYCN* and *let-7* expression are negatively correlated in non-amplified disease, underscoring the importance of *let-7* disruption in the absence of the *MYCN* ceRNA[34]. These data may collectively explain both preferential loss of certain *let-7* loci and common patterns of chromosomal loss in neuroblastoma.

Further underscoring the significance of *let-7* suppression is the observation that non-*MYCN*-amplified neuroblastoma patients had significantly worse overall survival (OS) if there was a *let-7* CN loss event (fig 5f top panel). In the rare case where *MYCN*-amplification and *let-7* CN loss occurred together, OS was dramatically reduced relative to the already poor-prognosis of *MYCN*-amplification (fig. 5f bottom panel), suggesting a deleterious synergy between two powerful but typically exclusive mechanisms of functional *let-7* disruption.

Of note, one of the tumors in the aCGH dataset had genetic amplification of *LIN28B* (CN=23, fig. 5a). This tumor patterned closely with *MYCN*-amplified tumors with regard to net *let-7* loss and tumor stage (IV) despite being 2n for *MYCN*. This may represent a case where *LIN28B* significantly contributed to neuroblastoma through *let-7* suppression similar to the reported mouse model of murine-*Lin28b* driven neuroblastoma[12].

Discussion

The known functionality of *LIN28B*, together with the patterns of genetic deletion of *let-7* and amplified *MYCN* ceRNA (aceRNA) activity described here establish that neuroblastoma employs multiple mechanisms to neutralize *let-7*, placing *let-7* disruption at the center of neuroblastoma pathogenesis. We thus propose that *let-7* biogenesis and function are targeted in neuroblastoma by several disparate mechanisms: high frequency genetic loss, *LIN28B* activity, or *MYCN* aceRNA (ED 10f). This model has implications for our understanding of neuroblastoma pathogenesis, disease modeling, and the rational design of therapeutic strategies, and may represent a more general feature of human cancer.

First, our model offers a plausible explanation for the uniquely high *MYCN* mRNA levels in amplified neuroblastoma, which enables both robust expression of MYCN protein and adequate copies of a ceRNA sufficient to impair the function of a highly expressed miRNA like *let-7*. Questions may remain about whether an observed >100 fold increase in *MYCN* mRNA, which increases the total *let-7* target-sites across the cellular pool of mRNAs by only approximately 25%, is sufficient to mediate a ceRNA effect on *let-7*. However, our functional data based on loss of the *MYCN* 3′UTR, including candidate reporter analysis of *let-7*-site-containing 3′ UTRs and global *let-7*-target mRNA-seq analysis (fig. 3d–g), suggest that *MYCN* mRNA may be a preferred target that in abundance can sequester and impair *let-7*. Further, in tumors lacking *MYCN* amplification, our model suggests that selective pressure to disrupt *let-7* explains the well known, yet unresolved, patterns of *MYCN*-amplification-independent chromosome 3p and 11q loss. AceRNA function of *MYCN* mRNA also accounts for the dispensability of *LIN28B* in *MYCN*-amplified cell lines, suggesting that *LIN28B* may serve a redundant *let-7* suppressive role.

Our findings suggest that highly expressed 3′UTRs contribute to miRNA deregulation in cancer, and therefore both coding and non-coding functions of oncogenic mRNAs should be considered in animal tumor modeling. For example, both the TH-*MYCN* and LSL-*MYCN;Dbh-iCre* models of murine neuroblastoma overexpresses the *MYCN* open reading frame and lack 3′UTRs. Notably, the TH-*MYCN* model has similar patterns of *let-7a2, let-7f2, and let-7g* genetic loss as non-amplified human disease and both models broadly downregulate the *let-7* family[34,41], further suggesting that *let-7* disruption is important even in the presence of *MYCN* protein expression. Moreover, a recent report demonstrates that high level expression of the *BRAF* pseudogene, which contains a functional 3′UTR but does not encode a protein, is sufficient to induce lymphoma in mice[42]. Consequently, full-length mRNA transgenes may yield more accurate genetic modeling of human tumors in animals.

Lastly, our model establishes *let-7* restoration as a key therapeutic goal in neuroblastoma. There are few neuroblastoma specific therapies, and attempts to directly target *MYCN* have

met with little success, despite efforts spanning the last 20 years[25,26,43]. The fact that *MYCN* mRNA has such a strong functional connection to *let-7* exposes a valuable opportunity to target *MYCN* itself and provides hope of delivering disease specific therapy to the worst prognostic class of neuroblastoma.

We show here that disparate modes of *let-7* suppression are selectively and inversely related in neuroblastoma. Given that both oncogenic amplification and disruption of *let-7* biogenesis appear to play central roles in multiple cancer types[15,44–47], our model may provide a novel organizing principle by which to consider and interrogate genetic events in a broad range of tumors.

Methods

Cell culture

BE(2)C (ATCC #CRL-2268), PA-1 (ATCC #CRL-1572), IMR90 (ATCC #CRL-186), SK-N-AS (ATCC #CRL-2137), SH-SY5Y (ATCC #CRL-2266), 293T(ATCC #11268), SK-N-DZ (ATCC #CRL-2149) and Kelly cells (Sigma #92110411-1VL) were maintained in 1:1 DMEM/F12:MEM media with 10% inactivated fetal calf serum, 1ug/ml penicillin, and 1U/ml streptomycin. All cell lines were purchased for the purposes of this study, are not among commonly misidentified cell lines (per ICLAC), and tested negative for mycoplasma contamination.

Plasmids

Turbo-RFP, *LIN28B*, and *MYCN*(ORF) cDNAs were subcloned into the pcDNA3.1 expression vector (Invitrogen). The *MYCN* 3′UTR was cloned from BE(2)C cDNA and subcloned into pcDNA3.1:*MYCN* to create pcDNA3.1:*MYCN*/3′UTR. ShRNA-resistant-*LIN28B* and pcDNA3.1:*MYCN*/3′UTR-*let-7*-site-mutant vectors were made using the QuikChange© site-directed-mutagenesis kit (Stratagene) on pcDNA3.1:*LIN28B* and pcDNA3.1:*MYCN*/3′UTR constructs, respectively. Wildtype and mutant *MYCN* 3′UTRs were subcloned into pcDNA3.1:*RFP* and psiCHECK2 to create pcDNA3.1:*RFP*/*MYCN*-3′UTRwt and pcDNA3.1:*RFP*/*MYCN*-3′UTRmut as well as psiCHECK2:*MYCN*wt and psiCHECK2:*MYCN*mut. pIS1:*DICER*1, pIS1:*IGF2BP1*, and pIS1:*Hmga2* were gifts from David Bartel[1,2] (Addgene plasmids #21649, #21639, and #14785). psiCHECK2-8x-let-7 was a gift from Yukihide Tomari[3] (Addgene plasmid #20931).

siRNA/let-7 mimic transfections

BE(2)C and Kelly cells were reverse transfected using Lipofectamine 2000© (Life Technologies) into 6 well plates using the appropriate siRNA or miRNA mimics (described below). Cells were harvested at time-points described for analysis by western or qPCR. Growth assays were performed similarly, but in 96 well plates followed by time-point specific BrdU growth assay. Global *let-7* target analysis: BE(2)C:*MYCN*-ORF cells co-transfected with control or *MYCN*-3′UTR-2 siRNA and either control or *let-7a* miRNA mimic were harvested 48 hours post transfection. Control siRNA (Life Technologies #439846). *LIN28B* siRNAs: ORF1 (Life Technologies #4392420, ID:s52479), ORF2 (Life

Technologies #4392420, ID:s52477), 5′UTR (GE Dharmacon Custom *LIN28B*-NM_001004317 Duplex siRNA, ON-TARGET Plus, sense: 5′-*ACU GGA GAG AGG AGA GAA AUU*-3′, antisense: 5′-*UUU CUC UCC UCU CUC CAG UUU*-3′), 3′UTR-1 (GE Dharmacon #J-028584-12-0020), 3′UTR-2 (GE Dharmacon Custom *LIN28B*-NM_001004317 Duplex siRNA, ON-TARGET Plus, sense: 5′-*CAA CAG UGA UUG UGA GAA UUU*-3′, antisense: 5′-*AUU CUC ACA AUC ACU GUU GUU*-3′). *MYCN* siRNAs: ORF-1 (Life Technologies #4392420, ID:s9135), ORF-2 (Life Technologies #4392420, ID:s9134). Control miRNA mimic (Life Technologies #4464059). *let-7a* miRNA mimic (Life Technologies #4464066, ID:MC10050), *let-7a* inhibitor (Life Technologies #4464084, ID:MH10050).

Luciferase Assays

For the *MYCN* 3′UTR loss of function assays, BE(2)C cells were reverse co-transfected using Lipofectamine 2000© in quadruplicate into 96-well plates with the appropriate luciferase vector and either control siRNA, *MYCN* siRNA or *let-7a* mimic. 60 hours post-transfection, luciferase activity was assayed using the Dual Luciferase© Reporter Assay System (Promega). For the *MYCN* 3′ UTR gain of function assays, 293T cells were seeded into 96-well plates in quadruplicate and transfected using Lipofectamine 2000© the following day with the appropriate luciferase vector, *MYCN* 3′UTR overexpression vector, and either control miRNA mimic or *let-7a* mimic. Luciferase activity was measured 24 hours post-transfection as described above.

Immunohistochemistry

Performed on human tumor tissue sections as previously described[4] using anti-LIN28B antibody (Cell Signaling #4196) at a 1:400 dilution. Patient samples were obtained through Boston Children's Hospital IRB-CRS08-09-0429-2; Immunohistochemical and Molecular Analysis of Pediatric Tumors and consent was obtained from all subjects.

Western blotting

Western blots were performed with antibodies against LIN28B (Cell Signaling #4196), LIN28A (Cell Signaling #3978), MYCN (Santa Cruz Biotechnology #sc-53993), DICER1 Santa Cruz #sc-30226), HK2 (Cell Signaling #2867S), IMP1 (Cell Signaling #2852S), tRFP (Origene #TA150061), β-TUBULIN (Cell Signaling #2146), and β-ACTIN (Santa Cruz Biotechnology #sc-8342).

BrdU growth assay

5000 cells per well were plated on a 96 well plate in quadruplicate for each of three independent experiments. Cell proliferation was assayed relative to day zero using the BrdU Cell Proliferation Assay Kit (Cell Signaling #6813) according to manufacturers protocol following two hour incubation with BrdU.

qPCR

Total RNA was isolated from cells using Trizol© reagent (Life Technologies). For mRNA analysis, cDNA was prepared from 1ug RNA using Superscript II© Reverse Transcriptase

(Life Technologies) and random hexamers. 20ng of cDNA was then used for qPCR with the SYBR© Select Master Mix (Life Technologies). mRNA primers: *LIN28B* (fwd: *GAG TCA ATA CGG GTA ACA GGA C*, rev: *CAC CAC AGT TGT AGC ATC TAT CT*) *MYCN*-1 (fwd: *CGA TTC AGA TGA TGA AGA TGA TGA AG*, rev: *GAC AGC CTT GGT GTT GGA*), *IGF2BP1* (fwd: *CAG TCC AAG ATA GAC GTG CAT AG*, rev: *CTC AGG GTT GTA AAG GGT AAG G*), *DICER1* (fwd: *CTC CTA CCA CTA CAA TAC TAT CAC T*, rev: *GGT CTT CAT AAA GGT GCT TGG T*), *β-ACTIN* (fwd: *GAC CCA GAT CAT GTT TGA GAC C*, rev: *CGT AGC ACA GCT TCT CCT TAA T*), *HMGA2* (fwd: *CTG CTC AGG AGG AAA CTG AAG*, rev: *CAC TAA ACC TGG GAC TGT GAA G*), *ARID3B* (fwd: *CAA GCA GAA TGG TGG TTT GG*, rev: *ATG GAT GTG GGC AGG TTT AG*). For *let-7* analysis, cDNA was prepared using 20ng total RNA and the Taqman© microRNA Reverse transcription kit (Life Technologies). 2ng cDNA was then used for qPCR with the Taqman© Universal PCR Master Mix (Life Technologies). Taqman© microRNA Assays used (Catalog #:4427975): *let-7a* (ID:000377), *let-7b* (ID:002619), *let-7c* (ID:000379) *let-7d* (ID:002283), *let-7e* (ID:002406), *let-7f* (ID:000382), *let-7g* (ID: 002282), *let-7i* (ID:002221), *miR-98* (ID: 000577), *U47* control microRNA Assay (ID:001223). For both mRNA and *let-7* expression analysis, relative expression was determined using the ΔΔCT method, unless otherwise noted.

qPCR CPC Analysis

Total RNA per cell was determined by RNA harvest yield from 1.5 x 10^6 cells. For *MYCN* mRNA copies per cell, cDNA was prepared using 200ng total RNA per cell type and from a dose curve of the synthetic *MYCN*-3′UTR-RNA-fragment (Integrated DNA Technologies) with Superscript III© Reverse Transcriptase (Life Technologies) and a *MYCN*-gene-specific primer (*MYCN*-2 rev). 10% of the cDNA reactions were then used for qPCR as described above. Linear regression analysis was performed on *MYCN*-3′UTR-RNA-fragment-sample CT values to determine the copies per reaction in the cell samples. *MYCN* mRNA copies per cell was then calculated based on the total RNA per cell previously determined. Synthetic *MYCN*-3′UTR-RNA-fragment sequence: (*5′-TTC CTA GCC TGT TTC TTC CTG TTA ATG TAT TTG TTC ATG TTT GGT GCA TAG AAC TGG GTA AAT GCA AAG TTC TGT GTT TAA TTT CTT CAA AAT GTA TAT ATT TAG TGC TGC ATC TTA TAG CAC TT -3′*). *MYCN*-2 qPCR Primers (fwd: *CCT AGC CTG TTT CTT CCT GTT A,* rev: *GTG CTA TAA GAT GCA GCA CTA AAT*). A similar strategy was used to determine let-7 copies per cell. Synthetic *let-7* RNA molecules for each *let-7* family member (Integrated DNA Technologies) were used in dose curves for cDNA reactions for each *let-7*. cDNA was prepared as described above, and 10% of cDNA reactions were used for qPCR as described above. Linear regression analysis of the synthetic-*let-7* qPCR CT values and total RNA per cell values were used to calculate copies per cell for each *let-7* family member.

RNA-Seq analysis

Copies per Cell Analysis: Sequence reads were aligned to the human transcriptome using HISAT version 0.1.6[5]. The transcriptome file used for polyA-RNA based libraries consisted of protein-coding and ncRNA sequences downloaded from ENSEMBL (release 80) ftp:// ftp.ensembl.org/pub/release-80/fasta/homo_sapiens/, as well as the ERCC control sequences. The transcriptome file used for short-RNA based libraries consisted of mature

microRNA sequences downloaded from mirBase (release 21: ftp://mirbase.org/pub/ mirbase/), in addition to the synthetic short RNA spike in oligonucleotides (Small RNA Spikes: LET7A2-5′SCR:/5Phos/rGrA rArGrA rUrGrU rGrGrU rGrUrU rGrUrA rUrArG rUrU, LET7I-5′SCR: 5′Phos-rGrG rUrArG rArUrA rGrUrU rGrUrU rGrUrG rCrUrG rUrU, MIR-NEG: 5′Phos-rUrU rArCrG rUrCrG rUrCrG rCrGrU rCrGrU rUrArU rU, MIR17-5′SCR: 5′Phos-rArU rCrGrC rCrUrG rArUrA rArArG rUrGrC rArGrG rUrArG, JP_MIR-NEG DH1: 5′Phos-rUrC rArCrA rArCrC rUrCrC rUrArG rArArA rGrArG rUrArG rA, JP_MIR-NEG DH2: 5′Phos-rUrU rGrUrA rCrUrA rCrArC rArArA rArGrU rArCrU rG)[6]. To estimate transcript abundances, we applied Salmon version 0.3.2[7] to the aligned reads and summarized transcript abundances into gene-level expression levels by summing all transcript expression levels mapping to the same gene. Gene-to-transcript mappings, and transcript type annotations were downloaded also from ENSEMBL (ftp:// ftp.ensembl.org/pub/release-80/gtf/homo_sapiens/). Unless otherwise stated, all RNA-Seq data is presented is Log10(1+TPM), which we refer to as Log(TPM) henceforth. In order to estimate the absolute copy number of transcripts per cell, we performed linear regression of the spike-in oligonucleotides concentration (Log10) on the Log(TPM) using the *lm* function in R for each sample. Using the slope and intercept estimated by this approach, we calculated the copies per cell of endogenous mRNA by determining the number of transcripts (based on Log(TPM) values) present in the total ng RNA used for library preparation. We then determined molecules per cell based on pre-determined pg RNA per cell. Global *let-7* target analysis: polyA-selected mRNA sequencing reads were processed as above, with no spike in RNAs used. RNA-seq datasets are available under GEO reference series GSE81500: (http://www.ncbi.nlm.nih.gov/geo/query/acc.cgi?acc=GSE81500).

Supplemental Methodology: spike controlled quantification of small RNA—
Through comparison to three miRNA spike-ins, including *let-7*-specific 5′-end-scrambled *let-7a* and *let-7i* spikes, we sought to minimize the effects of secondary structure bias known to exist during sRNA-seq library preparations, which can have significant effects on the relative efficiency of reads produced between different microRNAs[6] (ED 6). A total of six synthetic spikes were used. Disparate reads per million observed among the equimolar small RNA spikes (i.e. the miR-Neg, LET7A2, LET7I spikes have much higher read counts than equimolar MIR17, miRNegDH1, and miRNegDH2 spikes) demonstrate both the need to use spikes similar to the miRNA-of-Interest to accurately determine copies per cell and the risk inherent in using a single spike to determine copies per cell for all miRNAs. The use of multiple miRNA-specific spikes improves upon previous miRNA quantification strategies using a single control miRNA to quantify all miRNAs[8] by limiting potential disparate read efficiencies between a single spike and the miRNA of interest. Difficulty in calculation of relative expression of disparate miRNAs within a single dataset due to such variable read efficiencies can therefore be mitigated through the use of spike-ins that closely resemble each miRNA of interest.

CRISPR/Cas9

Cas9/gRNA co-expressing lentiviral constructs (lentiCRISPRv2) were generated and lentiviral particles were produced as previously described[9,10], using protocols and gRNA design tools from http://www.genome-engineering.org. Puromycin selection began twenty

four hours after lentiviral infection of BE(2)C and Kelly cells. Experiments were typically completed within three weeks of initial infection. Oligos used for gRNA cloning: *LIN28B* exon 2: (CAC CGC ATC GAC TGG AAT ATC AAA G, AAA CCT TGG ATA TTC CAG TCG ATG C). *LIN28B* exon 3.1: (CAC CGC AGA GCA AAC TAT TCA TGG A, AAA CTC CAT GAA TAG TTT GCT CTG C). *LIN28B* exon 3.2: (CAC CGA ATG ATT ACC TAT CTC CCT T, AAA CAA GGG AGA TAG GTA ATC ATT C). *LIN28B* exon 4: (CAC CGC CTT GTA GAT GCT ACA ACT G, AAA CCA GTT GTA GCA TCT ACA AGG C). Cas9/gRNA constructs: lentiCRISPRv2, lentiCRISPR:EGFPsgRNA-1, and lentiCRISPR:EGFPsgRNA-2, were gifts from Feng Zhang[9,10] (Addgene plasmids #52961, #51760, and #51761).

shRNA

Lentiviral particles were prepared as previously described[4]. pLKO.1 short hairpin expression constructs (Sigma Mission shRNA): *LIN28B* shRNAs (sh1: TRCN0000144508, sequence: 5′-CCTGTTTAGGAAGTGAAAGAA-3′; sh2: TRCN0000122599, sequence: 5′-GCCTTGAGTCAATACGGGTAA-3′). Control vector (SHC001:no insert).

Xenografts

BE(2)C and SK-N-DZ cells were infected with either SHC001 or TRCN0000122599 pLKO. 1 lentivirus, then puromycin selected for 48hrs. 1.5E6 infected cells were injected subcutaneously into female Rag2 knockout (c57bl/6, 8 weeks old) immune deficient mice. Three weeks post injection, mice were sacrificed and tumors were removed and weighed. This procedure is approved by the Boston Children's Hospital Institutional Animal Care and Use Committee under protocol #15-12-3071R, which limits xenograft tumor size to less than 2.0cm.

Array Comparative Genome Hybridization (aCGH) analysis

Preparation of the 202 neuroblastoma aCGH dataset has been previously described[11,12]. MicroRNA-containing loci were analyzed for gain or loss as previously described[13]. Statistical significance between *MYCN*-amplified and non-amplified tumors was determined using *t* test with Welch's adjustment on original copy number values. Kaplan-Meyer curve generation and analysis was done using GraphPad Prism software.

ENCODE RNA-Seq datasets

Mature *let-7* expression data for 12 cell types was obtained from whole cell small-RNA-Seq ENCODE/CSHL datasets and *let-7* host transcript expression data from 6 cell types was obtained from RNA-seq ENCODE datasets on the UCSC Genome Browser[14] (http://genome.ucsc.edu/). Expression levels were determined relative to *let-7c* and *let-7c* host transcript levels, respectively.

R2 Database

Human neuroblastoma patient microarray and RNA-seq datasets were obtained from the R2: microarray analysis and visualization platform (http://r2.amc.nl) and analyzed using

GraphPad Prism software. Significance was determined by *t* test with Welch's adjustment. Datasets used: Kozak (GEO ID: GSE45547), SEQC (GEO ID: GSE62564)

Statistical analysis

Unless otherwise noted, all experiments were performed at least three times independently. Statistical tests used are identified in each figure legend. P-values of less than 0.05 were considered significant.
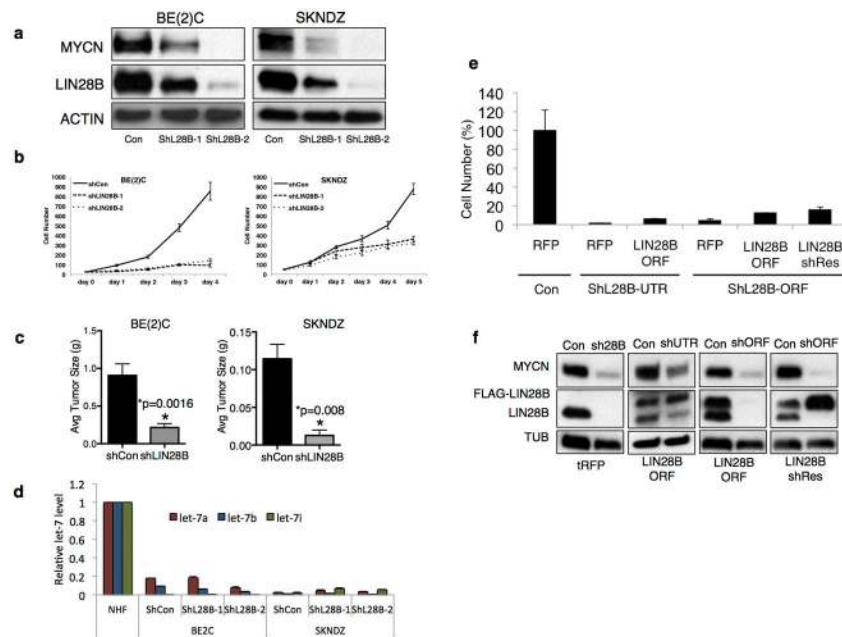
Extended Data
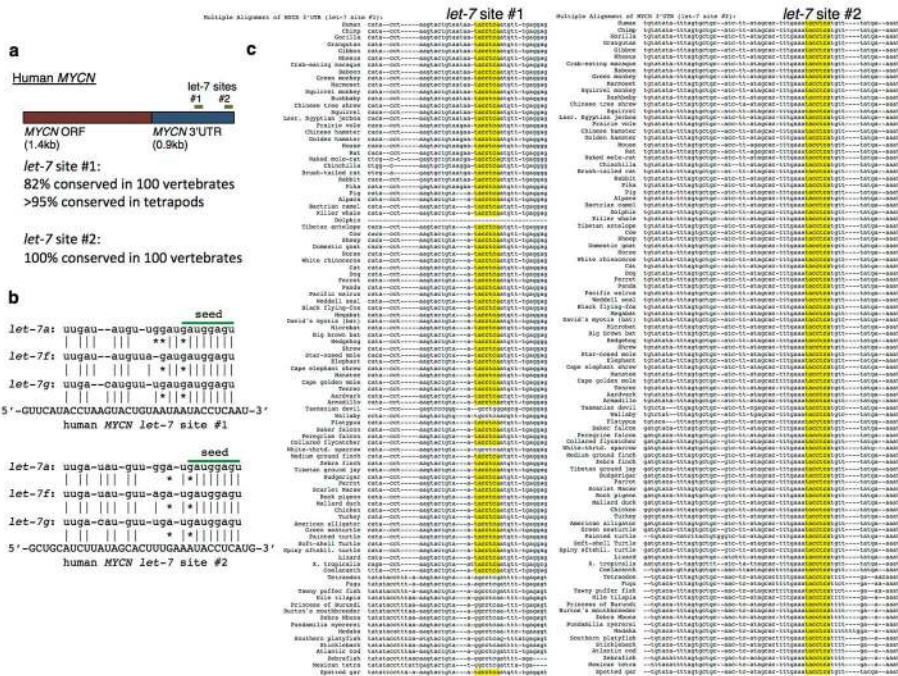
Extended Data 1. *MYCN* is a highly conserved let-7 target
(a) Schematic of human *MYCN* ORF and 3′UTR, indicating *let-7* sites 1 and 2 and their approximate location. (b) Predicted base pairing patterns of *let-7a*, *let-7f*, and *let-7g* with *MYCN* let-7 sites #1 and #2. A–G base pairs, common in RNA, are represented by (*). (c) Alignments of *let-7* sites 1 and 2 in 100 vertebrate *MYCN* 3′UTRs (ENCODE).
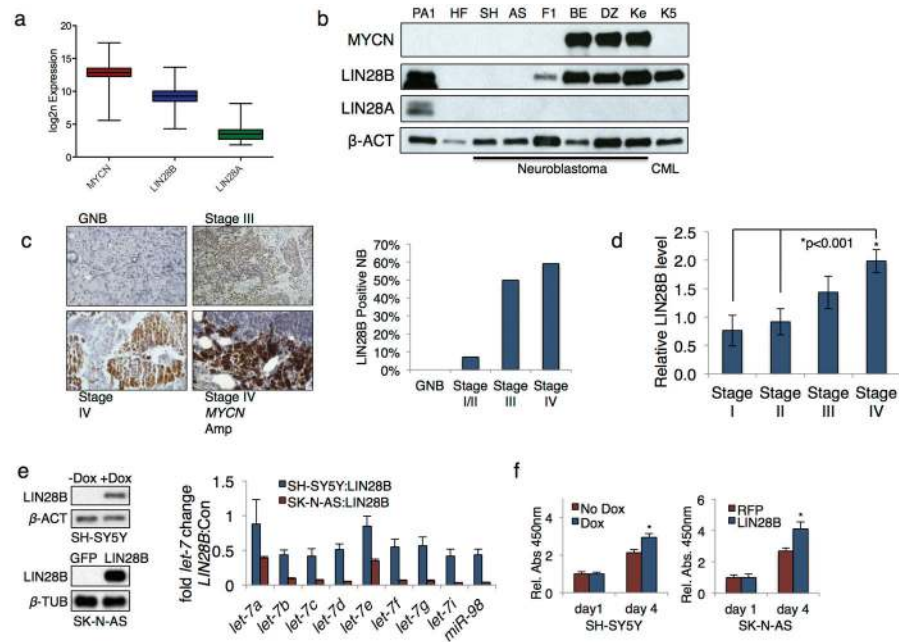
Extended Data 2. *LIN28B* expression and function in neuroblastoma

(a) *MYCN*, *LIN28B*, and *LIN28A* mRNA expression levels in neuroblastoma ($n = 649$, Source Data ED) (b) Immunoblot for indicated proteins in human embryonic carcinoma cells (PA1), normal human fibroblasts (HF), SK-N-SH (SH), SK-N-AS (AS), SK-N-F1 (F1), BE2C (BE), SK-N-DZ (DZ), Kelly (Ke), and human chronic myeloid leukemia cells (K5). For gel source data, see Supplemental Figures. (c) Representative LIN28B immunohistochemical staining of human neuroblastoma by stage (left panel), percent LIN28B positive neuroblastoma by disease stage (right panel). GNB = ganglioneuroblastoma. ($n = 36$) (d) *LIN28B* expression by neuroblastoma stage ($n = 64$, Source Data ED). (e) Immunoblot for LIN28B in inducible *LIN28B* SH-SY5Y cells and *GFP* or *LIN28B* expressing SK-N-AS cells (left panels) and corresponding qPCR analysis of relative *let-7* family levels (right panel), (mean plus s.e.m. of three independent experiments shown). (f) Relative growth rate (BrdU incorporation, right panel) of SH-SY5Y and SK-N-AS neuroblastoma cells from *d* (*p<0.05, $n = 3$ independent experiments).

Extended Data 3. Short hairpin knockdown of *LIN28B* in neuroblastoma

(a) Immunoblot for indicated proteins MYCN and LIN28B in *MYCN*-amplified cells infected with *LIN28B* targeting lentiviral shRNAs. For gel source data, see Supplemental Figures. (b) Cell proliferation analysis of cells described in *a*. (*n* = 3 independent experiments) (c) Average tumor size of human-mouse subcutaneous xenograft tumor analysis three weeks post injection of 2×10^6 cells infected with a *LIN28B* targeting lentiviral shRNA. (*n* = 6 mice for BE(2)C, *n* = 3 mice for SK-N-DZ, Supplemental Figures, Source Data ED). (d) qPCR analysis of *let-7a*, *let-7b*, and *let-7i* levels in cells described in *a*. (mean plus s.e.m. of three independent experiments shown) (e) Cell proliferation analysis of BE(2)C cells stably expressing red fluorescence protein (RFP), FLAG-tagged *LIN28B* ORF, or shRNA resistant FLAG-tagged *LIN28B* (LIN28B shRes) infected with *LIN28B* lentiviral shRNAs targeting the *LIN28B* 3′UTR (ShL28B-UTR) or the *LIN28B* open-reading frame (ShL28B-ORF). Cell counts were performed 7 days after lentiviral shRNA infection. (mean plus s.e.m. of three independent experiments shown) (f) Immunoblot for indicated proteins in cells described in *e*. For gel source data, see Supplemental Figures.
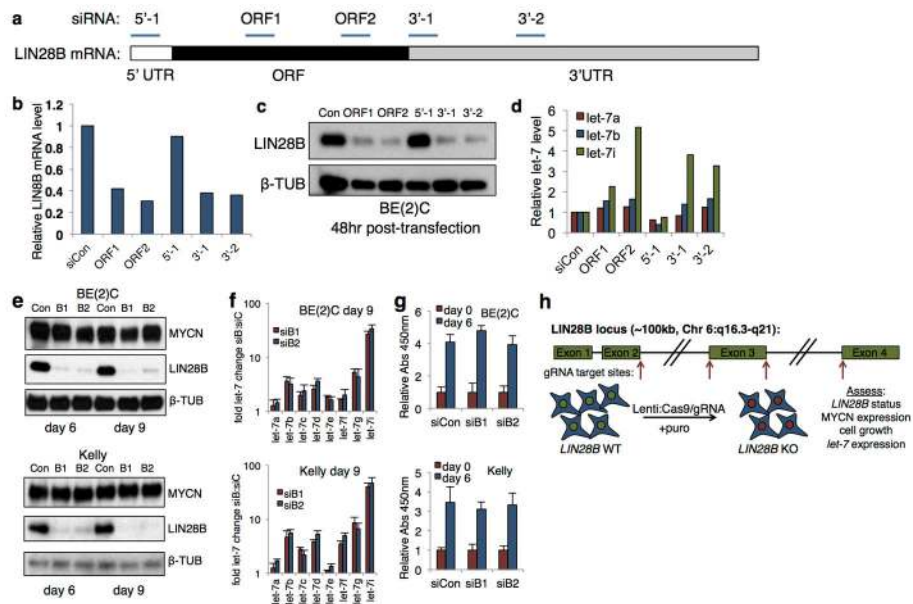
Extended Data 4. Small interfering RNA knockdown of *LIN28B* in neuroblastoma
(a) Schematic of approximate siRNA target sites within the *LIN28B* mRNA. (b) qPCR analysis of *LIN28B* mRNA levels in BE(2)C cell 48 hours after transfection with the indicated *LIN28B* targeting siRNAs. (mean of two independent experiments shown) (c) Immunoblot analysis of LIN28B in cells from *a*. For gel source data, see Supplemental Figures. (d) qPCR analysis of indicated *let-7* levels in cells from *a*. (mean of two independent experiments shown) (e) Immunoblot analysis of MYCN and LIN28B in serially transfected *MYCN*-amplified cells for 6 or 9 days. Identical transfections were performed of days 0, 3, and 6. For gel source data, see Supplemental Figures. (f) Day 9 qPCR analysis of the *let-7* family in the cells from *a*. (*n* = 3 independent experiments, mean plus s.e.m. shown) (g) Cell growth analysis of day 0 to day 6 cells from *a* (BrdU incorporation, *n* = 3 independent experiments, mean plus s.e.m. shown). (h) Lentiviral CRISPR-Cas9/*LIN28B* gRNA strategy targeting *LIN28B* at four distinct exon/intron junctions used in *b–g*.
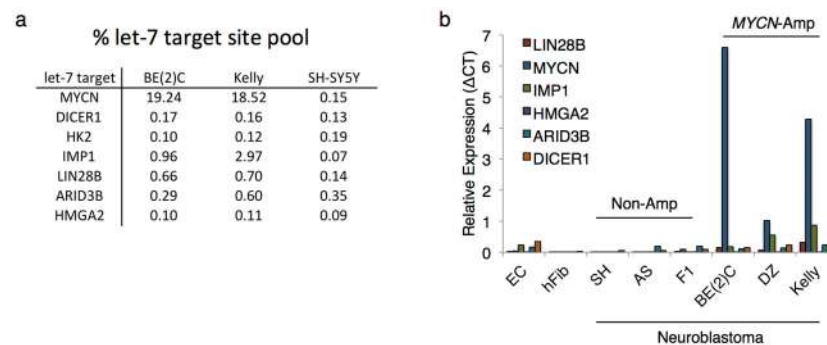
**Extended Data 5. Relative levels of *let-7* targets in neuroblastoma**
(a) mRNA-seq *let-7* target table (as percent *let-7* target site pool) (b) qPCR analysis of indicated let-7 targets in neuroblastoma cells, PA1 embryonic carcinoma cells (EC), and

normal human fibroblasts (hFib). Expression relative to *β-ACTIN* (ΔCT method) (mean of two biologic replicates shown).
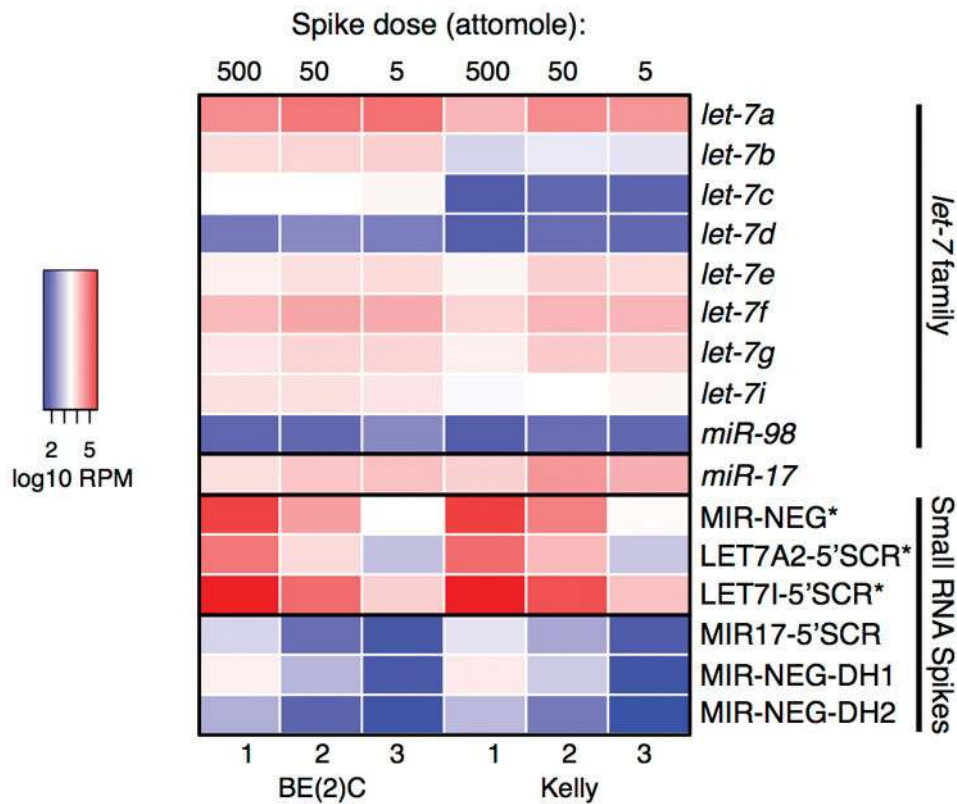
**Extended Data 6. Heat map of *let-7* and small RNA spike reads**
Heat map of three BE(2)C and three Kelly sRNA-seq samples depicting the relative reads per million of the *let-7* family, *miR-17*, and the six small RNA spikes added in equimolar amounts per sample (spikes miR-Neg, LET7A2, and LET7I were used to determine *let-7* copies per cell from the small RNA sequencing dataset). (RPM = reads per million).
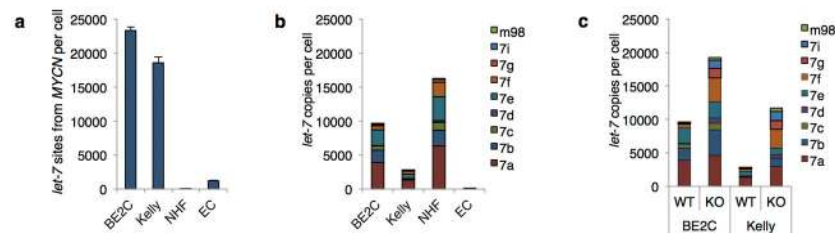
Extended Data 7. qPCR quantification of *MYCN* and *let-7* copies per cell
(a) Total *let-7* sites per cell provided by *MYCN* mRNA in BE(2)C, Kelly, normal human fibroblasts (NHF), and embryonic carcinoma cells (EC) (mean plus s.e.m. of 3 biologic replicates shown). (b) Total *let-7* copies per cell in cells from *a*, presented as stacked graphs of all let-7 family members (mean of 3 biologic replicates shown). (c) Total *let-7* CPC in wildtype or *LIN28B* knockout BE(2)C and Kelly cells, presented as stacked graphs of all

let-7 family members (values derived from let-7 CPC in *b* and average *let-7* fold change described in fig. 2f and 2*g*).
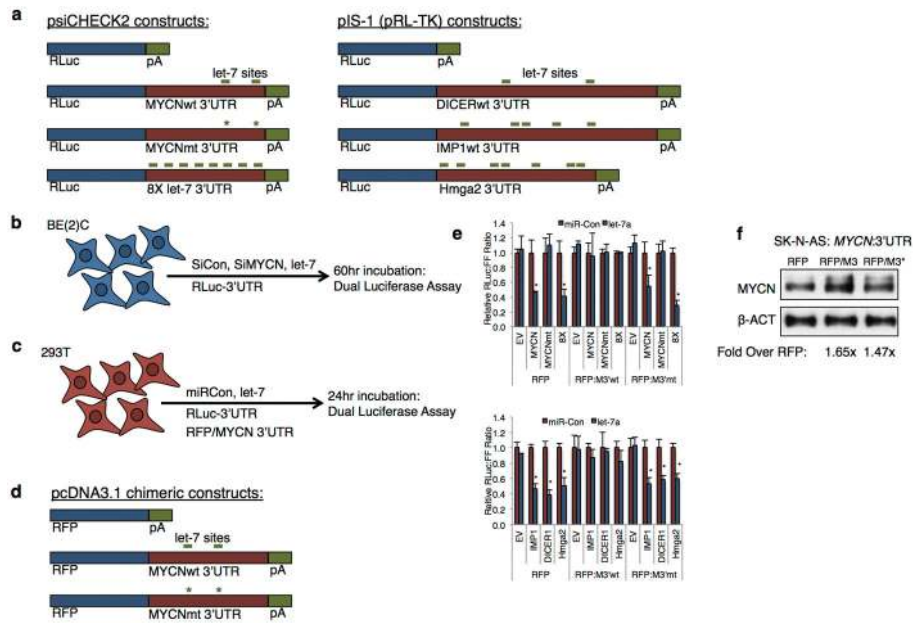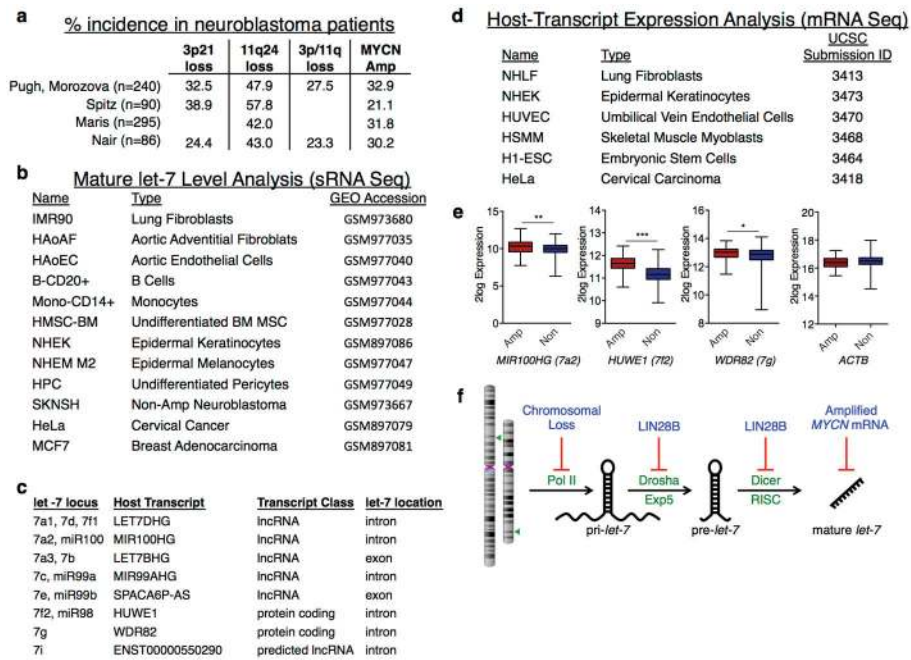

Extended Data 8. Luciferase reporter and gain of function constructs

(a) Luciferase constructs used in the luciferase assays in fig. 3d and ED 8e. (b) Schematic of the luciferase transfection protocols used in Figure 3d. (c) Schematic of the luciferase protocol used in *ED 8e*. (d) pcDNA3.1 constructs used in *ED 8e, 8f*. (e) Top panel: Relative luciferase ratio in 293T cells co-transected with the indicated 3′UTR luciferase and pcDNA3.1 vectors in the presence of either control miRNA or *let-7a* mimic. Bottom panel: Relative luciferase ratio in 293T cells co-transected with the indicated 3′UTR luciferase and pcDNA3.1 vectors in the presence of either a control miRNA or *let-7a* mimic. Mean of four independent experiments plus s.e.m. shown (*p<0.05 relative to E.V., unpaired t-test) (f) Immunoblot analysis of MYCN in SK-N-AS cell stably expressing a *MYCN* ORF+3′UTR transgene and transfected with the indicated pcDNA3.1 vector. For gel source data, see Supplemental Figures.
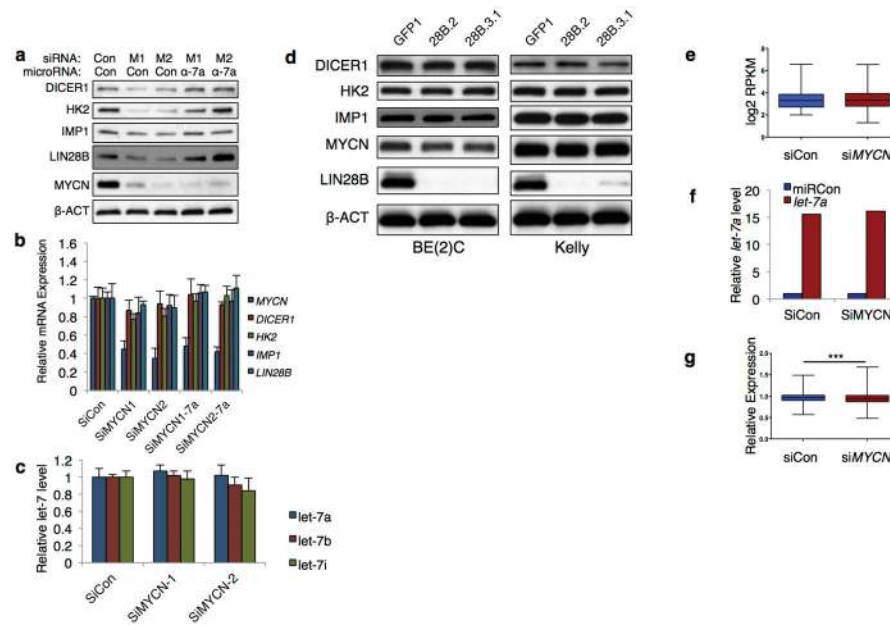
Extended Data 9. *MYCN* mRNA sponges *let-7*

(a) Immunoblot analysis of indicated proteins in BE(2)C cells transfected for 2.5 days with control, *MYCN-1* (M1), or *MYCN-2* (M2) siRNA and either control microRNA or *let-7a* inhibitor. For gel source data, see Supplemental Figures. (b) qPCR analysis of *DICER1*, *HK2, IMP1, LIN28B, and MYCN* in cells transfected as in *a.* (c) qPCR analysis of *let-7a*, *let-7b*, and *let-7i* in BE(2)C cells transfected for 2.5 days with control siRNA, siM1 or siM2. (*n* = 3 independent experiments, mean plus s.e.m. shown) (d) Immunoblot analysis of indicated proteins in cells infected with indicated Cas9-gRNA lentivirus. For gel source data, see Supplemental Figures. (e) Expression levels of *let-7* targets in BE(2)C:*MYCN* cells transfected with siCon or si*MYCN*-3′UTR. (f) Relative *let-7* expression in BE2C:*MYCN* cells co-transfected with siCon or si*MYCN* (3′UTR) siRNA and miRCon or *let-7a* mimic. A 16 fold increase in *let-7a* results in an approximately 8 fold increase in total *let-7*, due to *let-7a* making up almost half of the total cellular pool (fig. 3c, lower panel) (g) Relative expression levels of *let-7* targets in siCon and si*MYCN* cells transfected with *let-7a* mimic. (data represents one round of mRNA-seq, ***p<0.001, one-tailed Wilcoxon test, GSE81497, see Source Data F3).

a % incidence in neuroblastoma patients

	3p21 loss	11q24 loss	3p/11q loss	MYCN Amp
Pugh, Morozova (n=240)	32.5	47.9	27.5	32.9
Spitz (n=90)	38.9	57.8		21.1
Maris (n=295)		42.0		31.8
Nair (n=86)	24.4	43.0	23.3	30.2

b Mature let-7 Level Analysis (sRNA Seq)

Name	Type	GEO Accession
IMR90	Lung Fibroblasts	GSM973680
HAoAF	Aortic Adventitial Fibroblats	GSM977035
HAoEC	Aortic Endothelial Cells	GSM977040
B-CD20+	B Cells	GSM977043
Mono-CD14+	Monocytes	GSM977044
HMSC-BM	Undifferentiated BM MSC	GSM977028
NHEK	Epidermal Keratinocytes	GSM897086
NHEM M2	Epidermal Melanocytes	GSM977047
HPC	Undifferentiated Pericytes	GSM977049
SKNSH	Non-Amp Neuroblastoma	GSM973667
HeLa	Cervical Cancer	GSM897079
MCF7	Breast Adenocarcinoma	GSM897081

c

let-7 locus	Host Transcript	Transcript Class	let-7 location
7a1, 7d, 7f1	LET7DHG	lncRNA	intron
7a2, miR100	MIR100HG	lncRNA	intron
7a3, 7b	LET7BHG	lncRNA	exon
7c, miR99a	MIR99AHG	lncRNA	intron
7e, miR99b	SPACA6P-AS	lncRNA	exon
7f2, miR98	HUWE1	protein coding	intron
7g	WDR82	protein coding	intron
7i	ENST00000550290	predicted lncRNA	intron

d Host-Transcript Expression Analysis (mRNA Seq)

Name	Type	UCSC Submission ID
NHLF	Lung Fibroblasts	3413
NHEK	Epidermal Keratinocytes	3473
HUVEC	Umbilical Vein Endothelial Cells	3470
HSMM	Skeletal Muscle Myoblasts	3468
H1-ESC	Embryonic Stem Cells	3464
HeLa	Cervical Carcinoma	3418

Extended Data 10. Neuroblastoma patient and ENCODE data

(a) Detail of the incidence of chromosome 3p21 and 11q23 loss and *MYCN* amplification as determined by analysis of the indicated retrospective chromosomal aberration studies on neuroblastoma. (b) List of the ENCODE sRNA-seq samples analyzed (with associated GEO Accession numbers) for the relative expression of mature *let-7* in figure 5c. (c) List of *let-7* family host transcripts, transcript class, and *let-7* location within the transcript. (d) List of the ENCODE mRNA-seq samples analyzed (with associated UCSC Submission ID numbers) for the relative expression of *let-7* host-transcripts in figure 5d. (e) Relative expression of *let-7a2, let-7f2*, and *let-7g* host genes by microarray in *MYCN*-amplified and non-amplified neuroblastoma. *ACTB* shown as control. (*p<0.05, **p<0.01, ***p<0.001, unpaired *t-test*, $n = 643$, Source Data ED). (f) Schematic showing the several mechanisms that impair *let-7* biogenesis and function in neuroblastoma (chromosome images created at: http://www.ncbi.nlm.nih.gov/genome/tools/gdp/).

Supplementary Material

Refer to Web version on PubMed Central for supplementary material.

Acknowledgments

References

1. Croce CM. Causes and consequences of microRNA dysregulation in cancer. Nat Rev Genet. 2009; 10:704–14. [PubMed: 19763153]

2. Johnson SM, et al. RAS is regulated by the let-7 microRNA family. Cell. 2005; 120:635–647. [PubMed: 15766527]

3. Sampson VB, et al. MicroRNA let-7a down-regulates MYC and reverts MYC-induced growth in Burkitt lymphoma cells. Cancer Res. 2007; 67:9762–9770. [PubMed: 17942906]

4. Mayr C, Hemann MT, Bartel DP. Disrupting the pairing between let-7 and Hmga2 enhances oncogenic transformation. Science. 2007; 315:1576–9. [PubMed: 17322030]

5. Lu J, et al. MicroRNA expression profiles classify human cancers. Nature. 2005; 435:834–838. [PubMed: 15944708]

6. Boyerinas B, Park SM, Hau A, Murmann AE, Peter ME. The role of let-7 in cell differentiation and cancer. Endocr Relat Cancer. 2010; 17:F19–36. [PubMed: 19779035]

7. Gurtan AM, Sharp Pa. The role of miRNAs in regulating gene expression networks. J Mol Biol. 2013; 425:3582–600. [PubMed: 23500488]

8. Blandino G, et al. Tumor suppressor microRNAs: a novel non-coding alliance against cancer. FEBS Lett. 2014; 588:2639–52. [PubMed: 24681102]

9. Viswanathan SR, Daley GQ, Gregory RI. Selective blockade of microRNA processing by Lin28. Science. 2008; 320(80):97–100. [PubMed: 18292307]

10. Nguyen LH, et al. Lin28b is sufficient to drive liver cancer and necessary for its maintenance in murine models. Cancer Cell. 2014; 26:248–261. [PubMed: 25117712]

11. Viswanathan SR, et al. Lin28 promotes transformation and is associated with advanced human malignancies. Nat Genet. 2009; 41:843–848. [PubMed: 19483683]

12. Molenaar JJ, et al. LIN28B induces neuroblastoma and enhances MYCN levels via let-7 suppression. Nat Genet. 2012; 44:1199–206. [PubMed: 23042116]

13. Diskin SJ, et al. Common variation at 6q16 within HACE1 and LIN28B influences susceptibility to neuroblastoma. Nat Genet. 2012; 44:1126–30. [PubMed: 22941191]

14. Madison BB, et al. LIN28B promotes growth and tumorigenesis of the intestinal epithelium via Let-7. Genes Dev. 2013; 27:2233–45. [PubMed: 24142874]

15. Urbach A, et al. Lin28 sustains early renal progenitors and induces Wilms tumor. Genes Dev. 2014; 28:971–82. [PubMed: 24732380]

16. Tu HC, et al. LIN28 cooperates with WNT signaling to drive invasive intestinal and colorectal adenocarcinoma in mice and humans. Genes Dev. 2015; 29:1074–1086. [PubMed: 25956904]

17. Tay Y, Rinn J, Pandolfi PP. The multilayered complexity of ceRNA crosstalk and competition. Nature. 2014; 505:344–52. [PubMed: 24429633]

18. Poliseno L, et al. A coding-independent function of gene and pseudogene mRNAs regulates tumour biology. Nature. 2010; 465:1033–8. [PubMed: 20577206]

19. Cesana M, Daley GQ. Deciphering the rules of ceRNA networks. Proc Natl Acad Sci U S A. 2013; 110:7112–3. [PubMed: 23620514]

20. Lewis BP, Burge CB, Bartel DP. Conserved seed pairing, often flanked by adenosines, indicates that thousands of human genes are microRNA targets. Cell. 2005; 120:15–20. [PubMed: 15652477]

21. Melton C, Judson RL, Blelloch R. Opposing microRNA families regulate self-renewal in mouse embryonic stem cells. Nature. 2010; 463:621–6. [PubMed: 20054295]

22. Baeyens KJ, DeBondt HL, Pardi A, Holbrook SR. A curved RNA helix incorporating an internal loop with G z A and A z A non-Watson – Crick base pairing. Proc Natl Acad Sci U S A. 1996; 93:12851–12855. [PubMed: 8917508]

23. Pugh TJ, et al. The genetic landscape of high-risk neuroblastoma. Nat Genet. 2013; 45:279–84. [PubMed: 23334666]

24. Molenaar JJ, et al. Sequencing of neuroblastoma identifies chromothripsis and defects in neuritogenesis genes. Nature. 2012; 483:589–93. [PubMed: 22367537]

25. Barone G, Anderson J, Pearson ADJ, Petrie K. Europe PMC Funders Group New Strategies in Neuroblastoma: Therapeutic Targeting of MYCN and ALK. 2014; 19:1–12.

26. Maris JM. Recent advances in neuroblastoma. N Engl J Med. 2010; 362:2202–11. [PubMed: 20558371]

27. Seeger R, et al. Association of Multiple Copies of the N-Myc Oncogene with Rapid Progression of Neuroblastomas. N Engl J Med. 1983; 313:1111–16. [PubMed: 4047115]

28. Brodeur GM, Seeger RC, Schwab M, Varmus HE, Bishop JM. Amplification of N-myc in untreated human neuroblastomas correlates with advanced disease stage. Science. 1984; 224:1121–1124. [PubMed: 6719137]

29. Ala U, et al. Integrated transcriptional and competitive endogenous RNA networks are cross-regulated in permissive molecular environments. Proc Natl Acad Sci U S A. 2013; 110:7154–7159. [PubMed: 23536298]

30. Agarwal V, Stefano J, Bartel DP, Stoffel M. Article Assessing the ceRNA Hypothesis with Quantitative Measurements of miRNA and Target Abundance. Mol Cell. 2014; 54:766–776. [PubMed: 24793693]

31. Bosson AD, Zamudio JR, Sharp PA. Article Endogenous miRNA and Target Concentrations Determine Susceptibility to Potential ceRNA Competition. Mol Cell. 2014; 56:1–13. [PubMed: 25280098]

32. Agarwal V, Bell GW, Nam JW, Bartel DP. Predicting effective microRNA target sites in mammalian mRNAs. Elife. 2015; 4

33. Bartel DP. MicroRNA Target Recognition and Regulatory Functions. Cell. 2009; 136:215–233. [PubMed: 19167326]

34. Beckers A, et al. MYCN-targeting miRNAs are predominantly downregulated during MYCN-driven neuroblastoma tumor formation. Oncotarget. 2014; 6:5204–5216. [PubMed: 25294817]

35. Maris JM, et al. Allelic deletion at chromosome bands 11q14-23 is common in neuroblastoma. Med Pediatr Oncol. 2001; 36:24–27. [PubMed: 11464895]

36. Breen C, O'Meara a, McDermott M, Mullarkey M, Stallings R. Coordinate Deletion of Chromosome 3p and 11q in Neuroblastoma Detected by Comparative Genomic Hybridization. Cancer Genet Cytogenet. 2000; 120:44–49. [PubMed: 10913676]

37. EjeskÃ K. Loss of heterozygosity of 3p markers in neuroblastoma tumours implicate a tumour-suppressor locus distal to the FHIT gene. Br J Cancer. 1998; 77:1787–1791. [PubMed: 9667647]

38. Bray I, et al. Widespread dysregulation of MiRNAs by MYCN amplification and chromosomal imbalances in neuroblastoma: association of miRNA expression with survival. PLoS One. 2009; 4:e7850. [PubMed: 19924232]

39. Chiang HR, et al. Mammalian microRNAs: experimental evaluation of novel and previously annotated genes. Genes Dev. 2010; 24:992–1009. [PubMed: 20413612]

40. Roush S, Slack FJ. The let-7 family of microRNAs. Trends Cell Biol. 2008; 18:505–16. [PubMed: 18774294]

41. Hackett CS, et al. Genome-wide Array CGH Analysis of Murine Neuroblastoma Reveals Distinct Genomic Aberrations which Parallel those in Human Tumors Genome-wide Array CGH Analysis of Murine Neuroblastoma Reveals Distinct Genomic Aberrations which Parallel those in Human Tumo. 2004:5266–5273.

42. Karreth FA, et al. The BRAF Pseudogene Functions as a Competitive Endogenous RNA and Induces Lymphoma In Vivo. Cell. 2015; :319–332. DOI: 10.1016/j.cell.2015.02.043 [PubMed: 25843629]

43. Maris JM, Hogarty MD, Bagatell R, Cohn SL. Neuroblastoma. Lancet. 2007; 369:2106–20. [PubMed: 17586306]

44. Pugh TJ, et al. Exome sequencing of pleuropulmonary blastoma reveals frequent biallelic loss of TP53 and two hits in DICER1 resulting in retention of 5p-derived miRNA hairpin loop sequences. Oncogene. 2014; 33:5295–302. [PubMed: 24909177]

45. Rakheja D, et al. Somatic mutations in DROSHA and DICER1 impair microRNA biogenesis through distinct mechanisms in Wilms tumours. Nat Commun. 2014; 2:4802. [PubMed: 25190313]

46. Iwakawa R, et al. Genome-wide Identification of Genes with Amplification and / or Fusion in Small Cell Lung Cancer. 2013; 816:802–816.

47. Thériault BL, Dimaras H, Gallie BL, Corson TW. The genomic landscape of retinoblastoma: a review. Clin Experiment Ophthalmol. 2014; 42:33–52. [PubMed: 24433356]

48. Mayr C, Hemann MT, Bartel DP. Disrupting the pairing between let-7 and Hmga2 enhances oncogenic transformation. Science. 2007; 315:1576–9. [PubMed: 17322030]

49. Mayr C, Bartel DP. Widespread shortening of 3′UTRs by alternative cleavage and polyadenylation activates oncogenes in cancer cells. Cell. 2009; 138:673–84. [PubMed: 19703394]

50. Iwasaki S, Kawamata T, Tomari Y. Drosophila argonaute1 and argonaute2 employ distinct mechanisms for translational repression. Mol Cell. 2009; 34:58–67. [PubMed: 19268617]

51. Viswanathan SR, et al. Lin28 promotes transformation and is associated with advanced human malignancies. Nat Genet. 2009; 41:843–848. [PubMed: 19483683]

52. Kim D, Langmead B, Salzberg SL. HISAT: a fast spliced aligner with low memory requirements. Nat Methods. 2015; 12

53. Hafner M, et al. RNA-ligase-dependent biases in miRNA representation in deep-sequenced small RNA cDNA libraries. RNA. 2011; 17:1697–1712. [PubMed: 21775473]

54. Patro, R.; Duggal, G.; Kingsford, C. Salmon: Accurate, Versatile and Ultrafast Quantification from RNA-seq Data using Lightweight-Alignment. bioRxiv. 2015. at <http://biorxiv.org/content/early/2015/06/27/021592.abstract>

55. Bosson AD, Zamudio JR, Sharp PA. Article Endogenous miRNA and Target Concentrations Determine Susceptibility to Potential ceRNA Competition. Mol Cell. 2014; 56:1–13. [PubMed: 25280098]

56. Sanjana NE, Shalem O, Zhang F. Improved vectors and genome-wide libraries for CRISPR screening. bioRxiv. 2014; 11:006726.

57. Shalem O, et al. Genome-scale CRISPR-Cas9 knockout screening in human cells. Science. 2014; 343:84–7. [PubMed: 24336571]

58. Spitz R, et al. Oligonucleotide array-based comparative genomic hybridization (aCGH) of 90 neuroblastomas reveals aberration patterns closely associated with relapse pattern and outcome. Genes Chromosom Cancer. 2006; 45:1130–1142. [PubMed: 16958102]

59. Theissen J, et al. Chromosome 17 / 17q Gain and Unaltered Profiles in High Resolution Array-CGH are Prognostically Informative in Neuroblastoma. 2014; 649:639–649.

60. Rushlow DE, et al. Characterisation of retinoblastomas without RB1 mutations: genomic, gene expression, and clinical studies. Lancet Oncol. 2013; 13:327–34. [PubMed: 23498719]

61. Kent WJ, et al. The Human Genome Browser at UCSC The Human Genome Browser at UCSC. Genome Res. 2002; 12:996–1006. [PubMed: 12045153]
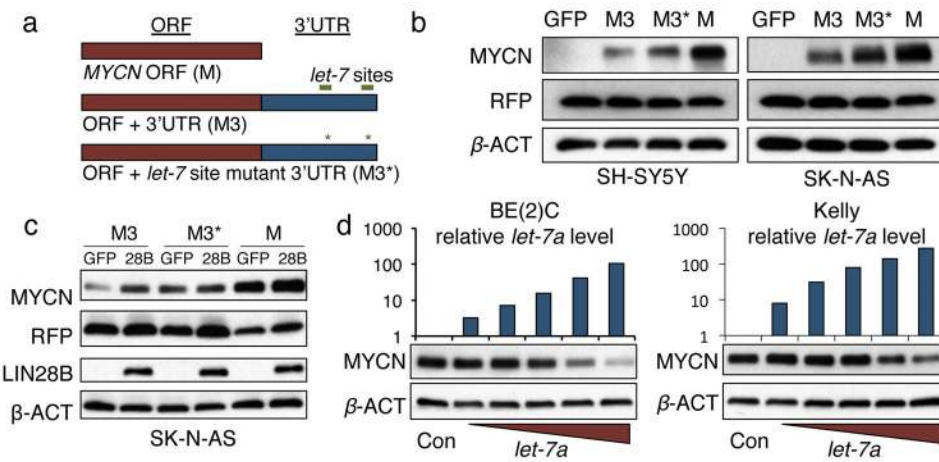
Figure 1. The *LIN28B/let-7/MYCN* axis is intact in neuroblastoma

(a) pcDNA3.1:*MYCN* constructs. (b) Immunoblot for indicated proteins in non-*MYCN*-amplified neuroblastoma cells transfected indicated constructs. (c) Immunoblot for indicated proteins in *GFP* or *LIN28B* expressing cells transfected as in *b*. (d) qPCR analysis of *let-7a* levels and immunoblot for MYCN in *MYCN*-amplified cells transfected with control or *let-7a* mimic dose curve (data representative of 3 independent experiments). For gel source data, see Supplemental Figures.
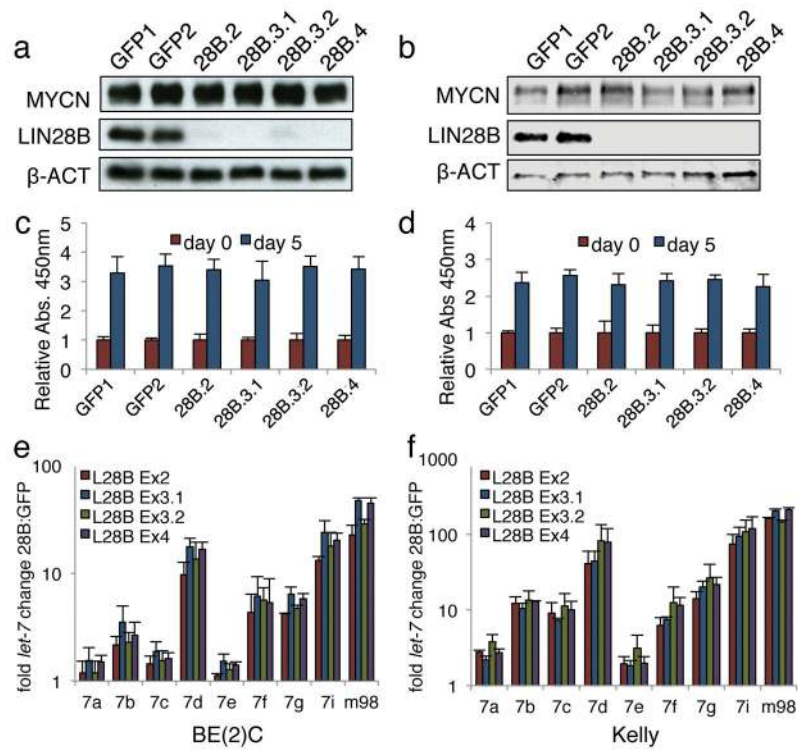
Figure 2. *LIN28B* is dispensable in human *MYCN* amplified neuroblastoma cells
(a,b) Immunoblot for MYCN and LIN28B in cells infected with indicated Cas9-gRNA lentivirus. For gel source data, see Supplemental Figures. (c,d) Cell growth analysis of cells infected as in *b, c.* (BrdU incorporation). (e,f) qPCR analysis of relative *let-7* expression in cells from *b*, and *c* respectively. Fold change relative to GFP gRNA controls. ($n = 3$ independent experiments, mean + standard error of the mean (s.e.m.) shown).
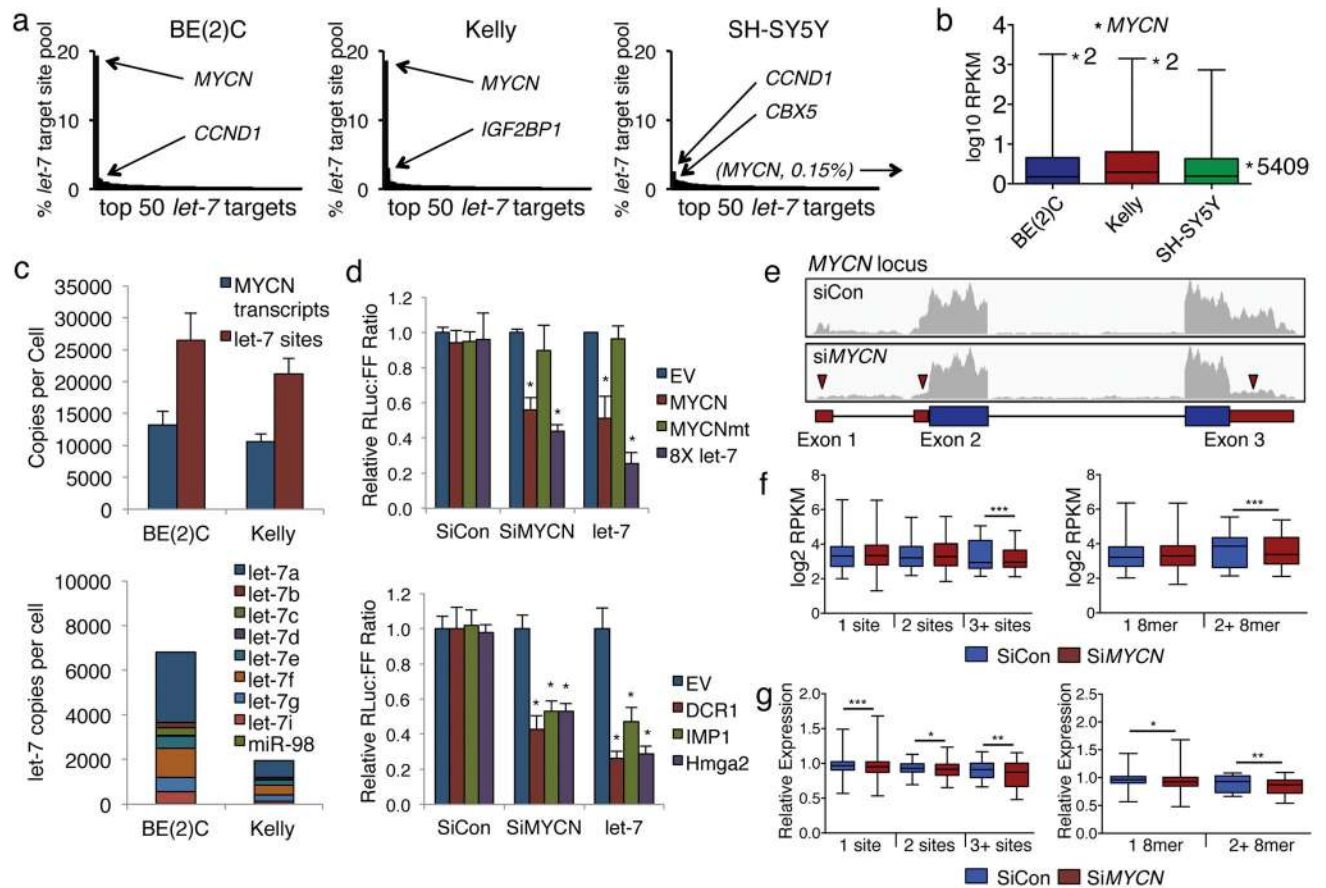
Figure 3. *MYCN* mRNA is an amplified competing endogenous RNA (aceRNA) for *let-7*
(a) *Let-7*-target-site-pool contribution of the top 50 targets. Arrows indicate top two contributors (*n* = 3 biologic replicates, GSE81498, see Source Data F3). (b) Box and whisker plot of top 14,000 expressed mRNAs from dataset described in *a*. *MYCN* expression rank marked by asterisk (GSE81498, see Source Data F3). (c) Top panel: *MYCN* transcripts and *let-7*-sites-provided per cell as determined by the dataset from *a*. (mean + standard deviation from the mean (s.d.) shown, GSE81498, see Source Data F3) Lower panel: *let-7* copies per cell as determined sRNA-seq (*n* = 3 biologic replicates, GSE81499, see Source Data F3). (d) Top Panel: Relative fluorescence ratio in BE(2)C cells co-transected with indicated constructs small RNAs. Bottom panel: Relative fluorescence ratio in cells co-transfected with indicated constructs and small RNAs. Mean of four independent experiments plus s.e.m. (*p<0.05 relative to E.V., unpaired t-test) (e) mRNA-seq reads mapping to the *MYCN* locus in BE(2)C:MYCN cells transfected with indicated siRNAs. Blue and red boxes indicate *MYCN* ORF and UTRs, respectively. Triangles mark reduction of *MYCN* mRNA untranslated regions. (f) Expression levels of mRNAs with 1, 2, or 3+ *let-7* sites (left panel) or with 1 or 2+ 8mer *let-7* sites (right panel) in siCon and si*MYCN* cells (data represents one round of mRNA-seq, ***p<0.0001, one-tailed Wilcoxon test). (g) Relative expression of mRNAs with 1, 2, or 3+ *let-7* sites (left panel) or with 1 or 2+ 8mer *let-7* sites (right panel) in siCon and si*MYCN* cells co-transfected with *let-7a*. Values

relative miRCon. (data represents one round of mRNA-seq, *p<0.05, **p<0.001, ***p<0.001 *vs.* siCon, one-tailed Wilcoxon test, GSE81497, see Source Data F3).
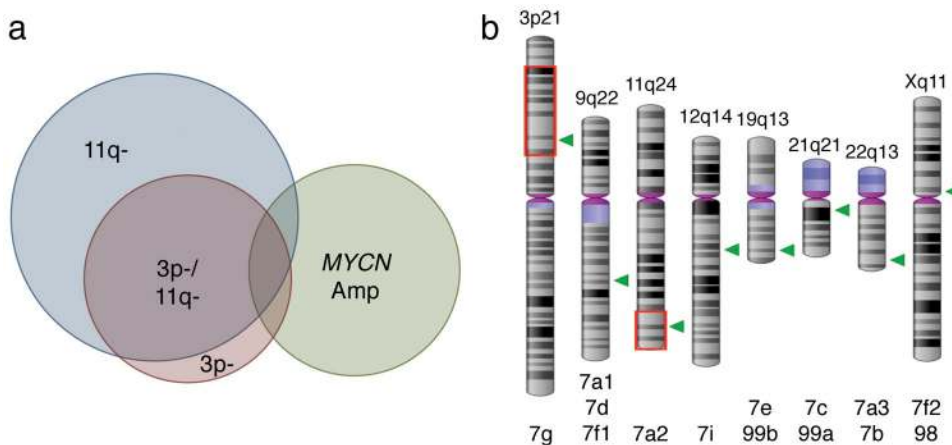
Figure 4. *Let-7a2* and *let-7g* are commonly lost in neuroblastoma

(a) Scaled Venn diagram assembled from Pugh, *et. al.*, (2013) detailing relative incidence and intersection of chromosome 11q and 3p loss and *MYCN* amplification.. (b) Genetic locations of 12 distinct *let-7* family members. Green triangles *let-7* loci. Red boxes indicate the SRO for these deletions. (Images created at: http://www.ncbi.nlm.nih.gov/genome/tools/gdp/).
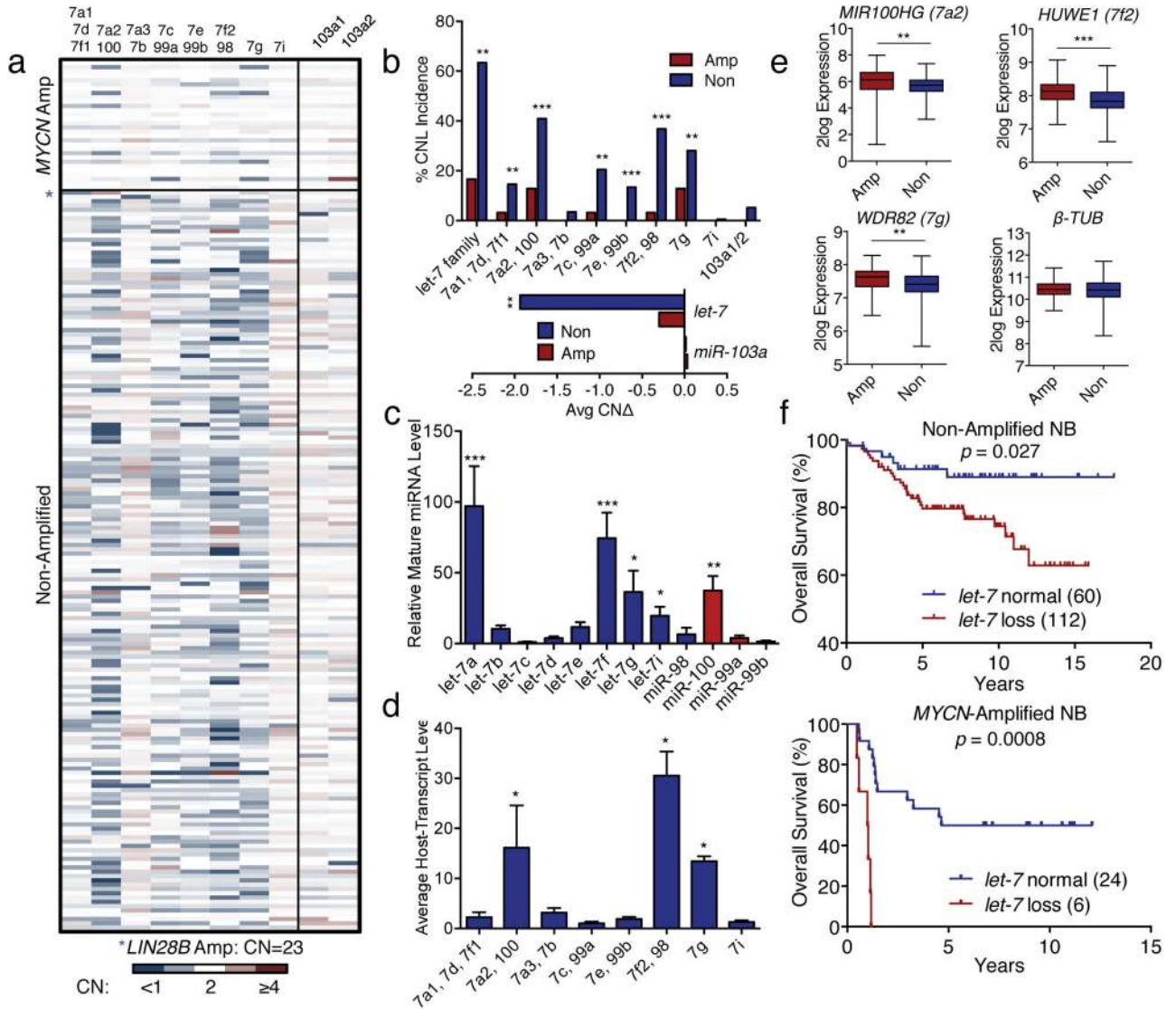
Figure 5. The *MYCN* aceRNA model predicts *let-7* chromosomal loss patterns in neuroblastoma
(a) *let-7* and *miR-103a* loci CN heat map based on aCGH relative fluorescence ratios of tumor *vs.* germline. (Source Data F5). (b) CN loss incidence for *let-7* and *miR-103a* from dataset in *a* (upper panel). Average CN change for the two miRNA families (lower panel). (*p<0.05, **p<0.01, ***p<0.001 amp vs. non for each locus, unpaired t-test, Source Data F5) (c) Mature *let-7* expression based on ENCODE sRNA-seq data. (*p<0.05, **p<0.01, ***p<0.001 *vs. let-7c*, Wilcoxon test, Source Data F5) (d) Relative *let-7* host transcript levels based on ENCODE mRNA-seq data. (*p<0.05, **p<0.01 *vs. let-7c*, Wilcoxon test, Source Data 3) (e) Relative expression of indicated host genes in *MYCN*-amplified and non-amplified neuroblastoma. *β-TUB* shown as control. (*n* = 498, **p<0.01, ***p<0.001, unpaired *t-test*, Source Data F5). (f) Overall survival curves of neuroblastoma patients in non-amplified (top panel), and *MYCN*-amplified (bottom panel) neuroblastoma. p-values determined by Mantel-Cox test (Source Data F5).